Supporting Information

Constructing electron transfer channel *via* Cu-O-Ni to inhibit the overoxidation of Ni for durable methanol oxidation at industrial current density

Han Tian[#], Xiaohan Wang[#], Wenshu Luo, Rundong Ma, Xu Yu, Shujing Li, Fantao Kong, Xiangzhi Cui, and Jianlin Shi*

H. Tian, X. Wang, W. Luo, R. Ma, X. Yu, F. Kong, X. Cui, J. Shi

Shanghai Institute of Ceramics, Chinese Academy of Sciences, Shanghai 200050, China.

X. Wang, S. Li, X. Cui

School of Chemistry and Materials Science, Hangzhou Institute for Advanced Study, University of Chinese Academy of Sciences.

X. Wang, W. Luo, X. Yu, X. Cui, J. Shi

Center of Materials Science and Optoelectronics Engineering, University of Chinese Academy of Sciences, Beijing 100049, P.R. China

Email: cuixz@mail.sic.ac.cn

[#]These authors contributed equally to this work.

Experimental Section

1. Materials

Except noted, all chemicals were purchased and used without further purification. Deionized water was used throughout the experiments. Copper (II) Chloride Dihydrate ($CuCl_2 \cdot 2H_2O$, 99%) was obtained from General-Reagent. Nickel (II) chioride hexahydrate ($NiCl_2 \cdot 6H_2O$, 99%), sulfuric acid (H_2SO_4, 99%), hydrochloric acid (HCl) and potassium hydroxide (KOH, 85%) were acquired from Sinopharm Chemical Reagent Co., Ltd. Methyl Alcohol (CH_3OH, 99.5%), formic acid (CH_2O_2, 98%), deuterium oxide (D_2O, 99.9%) and maleic acid ($C_4H_4O_4$, 99%) were all obtained from Adamas-beta.

2. Synthesis of Ni/NF

Nickel foam (NF) was used as matrix for growing Ni. Before the electrodeposition process, NF (10 × 20 × 1.5 mm) was ultrasonically cleaned by HCl, ethanol and deionized water for about 10 min to get rid of the possible surface dirt and oxide layer. Typically, 0.4 M $NiCl_2 \cdot 6H_2O$ were dissolved in a mixed solution of 5 mL H_2SO_4 and 95 mL deionized water under stirring to form a homogeneous solution. Then NF was electrodeposited in a mixed solution for 20,000 s at -150 mA. The substrate was taken out and cleaned by deionized water and ethanol several times before being fully dried at 100 °C for 12 h under air atmosphere, Ni/NF was obtained.

3. Synthesis of CuO_x/NF

To synthesize CuO_x/NF, the pretreated NF (10 × 20 × 1.5 mm) was electrodeposited in a deionized aqueous solution (100 mL) containing 0.4 M $CuCl_2 \cdot 6H_2O$ and 5 ml H_2SO_4 for 2000 s, and final drying at 100 °C for 12 hours under air atmosphere.

4. Synthesis of $NiCuO_x$-1/NF, $NiCuO_x$-2/NF and $NiCuO_x$-3/NF

To synthesize $NiCuO_x$-2, the pretreated NF (10 × 20 × 1.5 mm) was electrodeposited in deionized aqueous solution (100 mL) containing 0.4 M $NiCl_2 \cdot 6H_2O$ and 5 mL H_2SO_4 for 20,000 s, and then electrodeposited in deionized aqueous solution (100 mL)

containing 0.4 M $CuCl_2 \cdot 6H_2O$ and 5 mL H_2SO_4 for 2000 s, and final drying at 100 °C for 12 hours under air atmosphere. In addition, samples with electrodeposited copper source times of 1000 and 4000 s were prepared and named as $NiCuO_x$-1/NF and $NiCuO_x$-3/NF, respectively.

5. Materials Characterization

The scanning electron microscope (SEM) measurements were performed on a FEI Magellan-400 field emission scanning electron microscope (5 kV). The transmission electron microscopic (TEM) images, high-resolution TEM (HRTEM) and corresponding energy dispersive X-ray spectrometer mapping (EDS-mapping) were captured on a 200 kV JEOL JEM-F200 transmission electron microscope operated with a field-emission electron gun. The X-ray diffraction (XRD) patterns were acquired from the Rigaku D/Max-2550V X-ray diffractometer with a Cu K_α radiation target (40 kV, 40 mA) at a scan rate of 4 ° min^{-1}. The X-ray photoelectron spectroscope (XPS) signals were measured on a Thermo Fisher Scientific ECSA lab 250 XPS spectrometer with monochromatic Al K_α X-rays and calibrated with carbon base (284.8 eV).

6. Electrochemical measurements

All electrochemical measurements were performed with the biologic VSP-300 and CHI 760E electrochemical workstation in a standard three-electrode set-up at room temperature. The as-prepared Ni foam supported CuO_x, Ni, $NiCuO_x$-1, $NiCuO_x$-2 and $NiCuO_x$-3 catalysts with geometrical area of 0.25 cm^2 were directly used as the working electrode with a carbon rod counter electrode and saturated calomel electrode (SCE) electrode as the reference electrode. The electrolytes for OER process and MOR process were 1.0 M KOH and 1 M KOH with 1 M MeOH, respectively. According to the Nernst equation, the potential data reported in this work were converted to the reversible hydrogen electrode (RHE) scale: E (*vs.* RHE) = E (*vs.* SCE) + 0.244 + 0.0591 × pH. The scan rates of LSV and CV were kept at 5 and 10 mV s^{-1}, respectively. The Tafel slopes were derived from LSV curves.

Operando EIS measurements were conducted over a frequency range from 10^{-2} to

10^5 Hz with AC amplitude of 5 mV. All the curves are used without iR compensation if not labeled.

The measurement of multipotential steps were performed on $NiCuO_x$-2/NF during MOR and OER. First, the initial applied potential was set to 1.62 V (vs. RHE) for 30 s. Then, the applied potential was switched to 0.57 V (vs. RHE) after entering an open-circuit state for 90 s. Correspondingly, the red, blue and black lines are connected with condition I (with 1 M MeOH addition), condition II (without 1 M MeOH addition) and condition III (inject 1 M MeOH at 30 s), respectively.

7. Methanol valorization and products analysis

The analysis of liquid products from methanol valorization was performed by ^1H nuclear magnetic Resonance (HNMR) spectroscopy on an Avance II 500 instruments (Bruker). Long-term electrolysis reactions were carried out at varied potentials for 1 h by chronoamperometry testing in 80 mL electrolyte of 1 M KOH with 1 M methanol. For each NMR measurement, 500 μL electrolyte was added into a 100 μL D_2O solution with maleic acid as internal standard. The composition of electrolyte after methanol oxidation was identified based on the chemical shift of ^1H NMR. The product concentration was determined by the calibration curves of standard solution with given concentrations. The yield rate of formate and product Faradaic efficiency were calculated by the following equations:

$$Formate\ generation = \frac{C_{formate} \times V}{t \times M_{formate}}$$

$C_{formate}$ is the measured formate concentration (g L^{-1}) in the solution from the anode compartment of the cell, namely, the HNMR data. V is the volume of electrolyte (0.08 L), M formate (g mol^{-1}) is the molecular weight of formate ($HCOO^-$) equal to 45.02 g mol^{-1}, and t is the electrolysis time (1 h).

$$FE(\%) = \frac{n \times 4 \times N_A \times e}{Q} \times 100\%$$

where n is the mol of generated formate; 4 is the number of transferred electrons; N_A is Avogadro constant (6.02×10^{23} mol^{-1}); e is elementary charge (1.60×10^{-19} C); Q is

the passed charge (C).

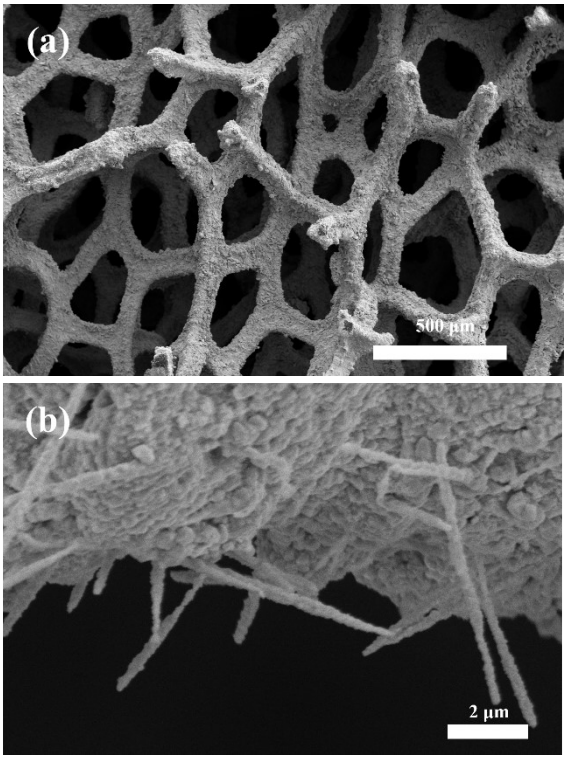

Figure S1. SEM images of the as-synthesized $NiCuO_x$-1/NF at different magnifications.

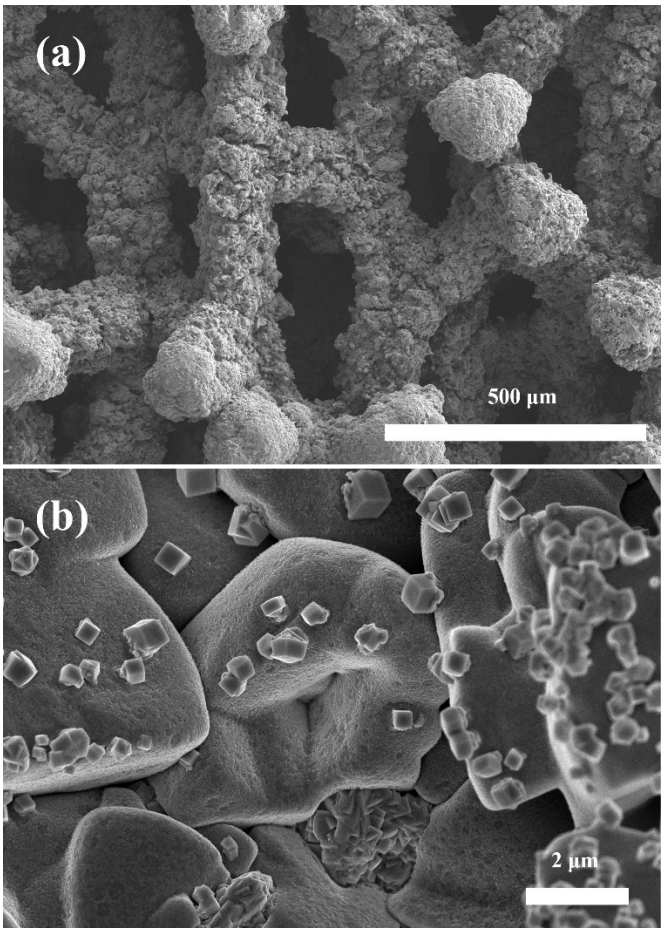

Figure S2. SEM images of the as-synthesized $NiCuO_x$-3/NF at different magnifications.

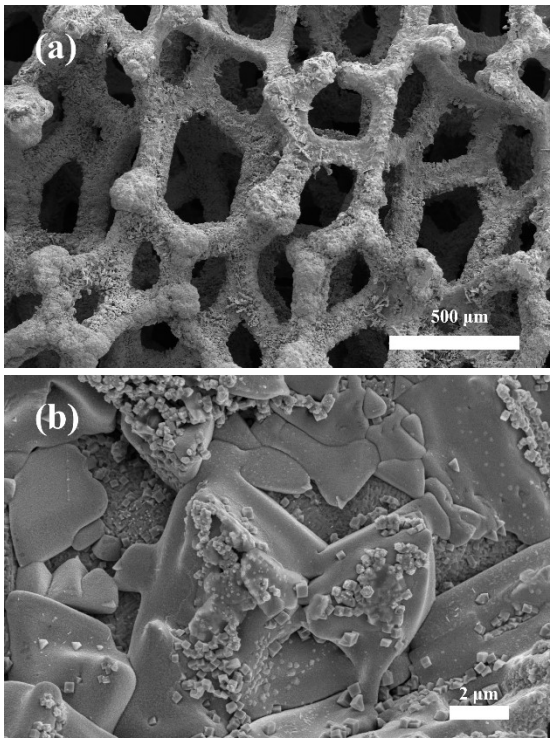

Figure S3. SEM images of the as-synthesized CuO_x/NF at different magnifications.

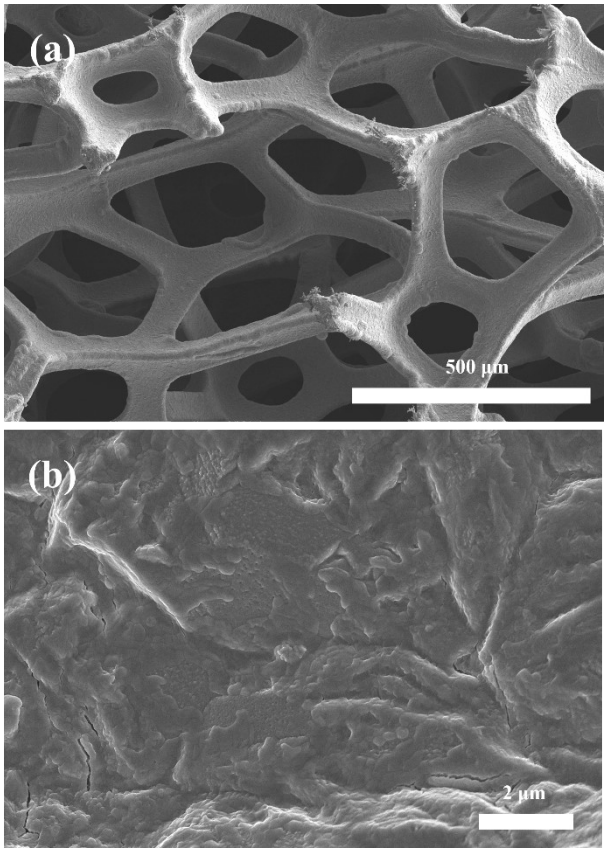

Figure S4. SEM images of the as-synthesized Ni/NF at different magnifications.

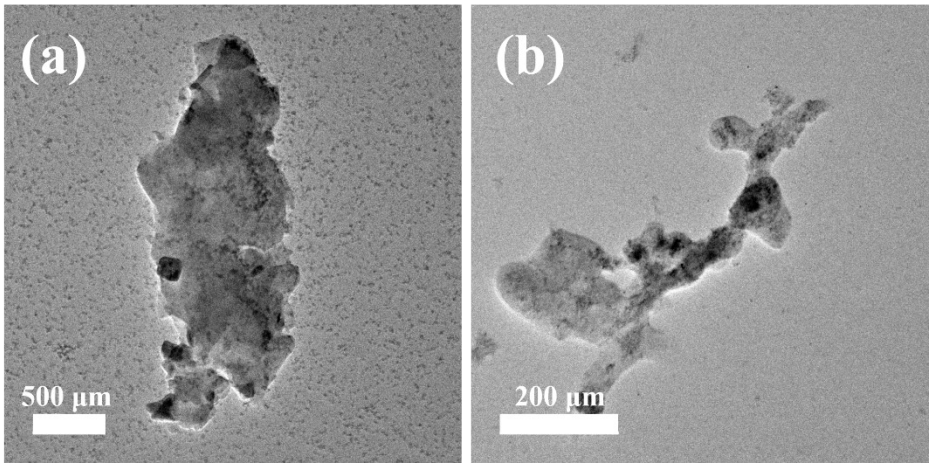

Figure S5. TEM images of the as-synthesized (a) CuO_x/NF and (b) Ni/NF.

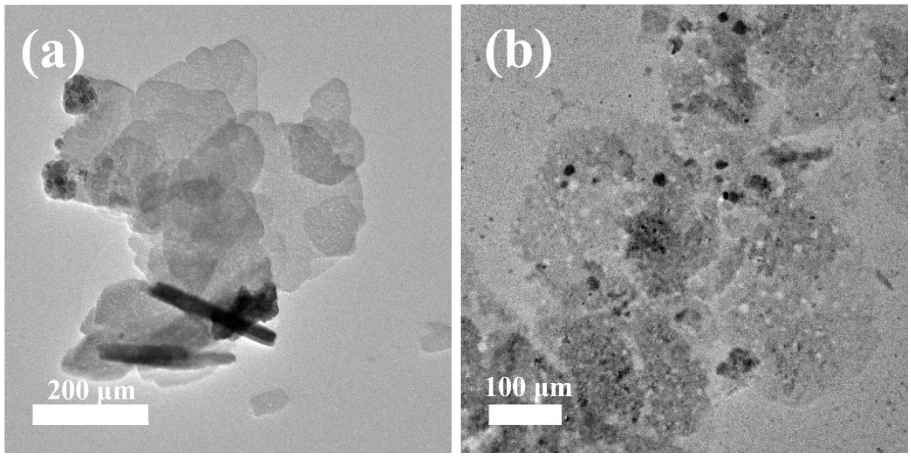

Figure S6. TEM images of the as-synthesized (a) $NiCuO_x$-1/NF and (b) $NiCuO_x$-3/NF.

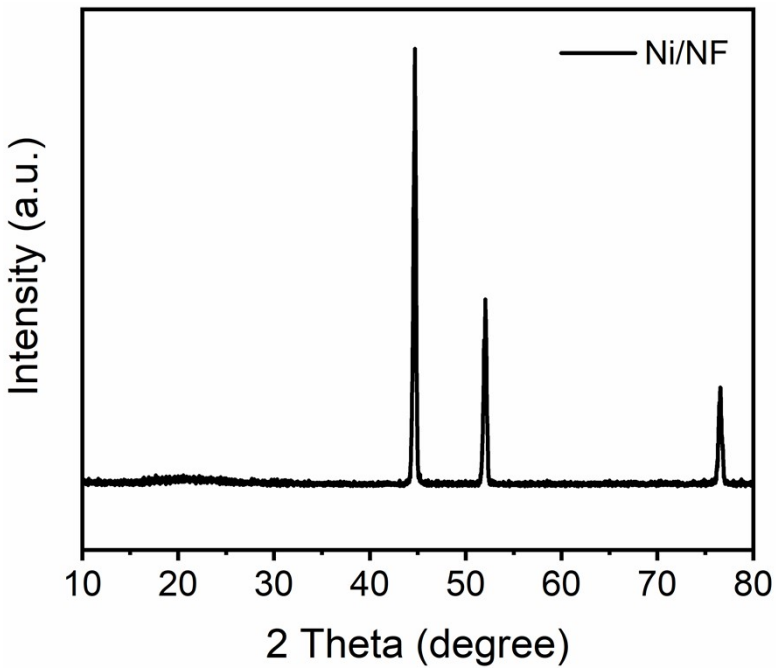

Figure S7. XRD patterns of the as-synthesized Ni/NF.

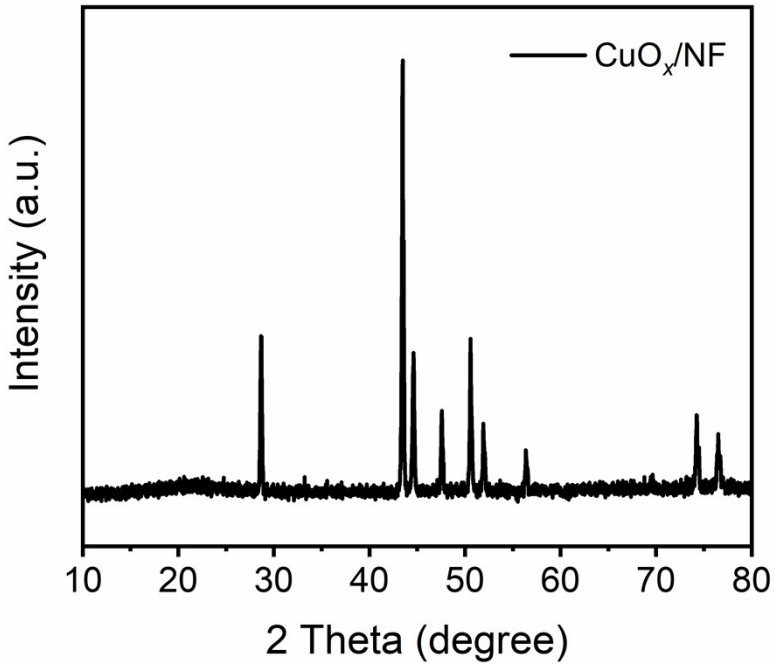

Figure S8. XRD patterns of the as-synthesized CuO_x/NF.

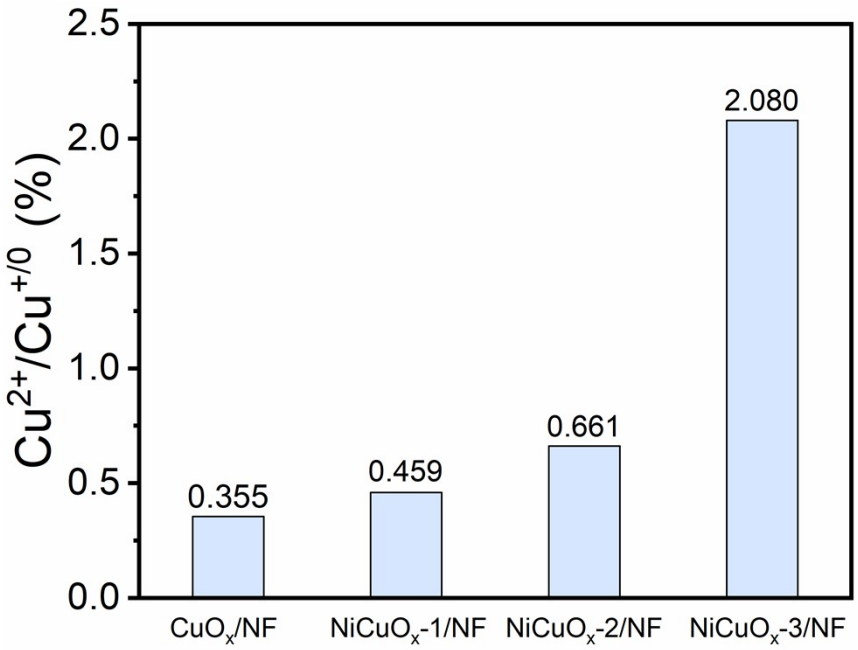

Figure S9. Histograms of $Cu^{2+}/Cu^{+/0}$ ratio for as-prepared catalysts.

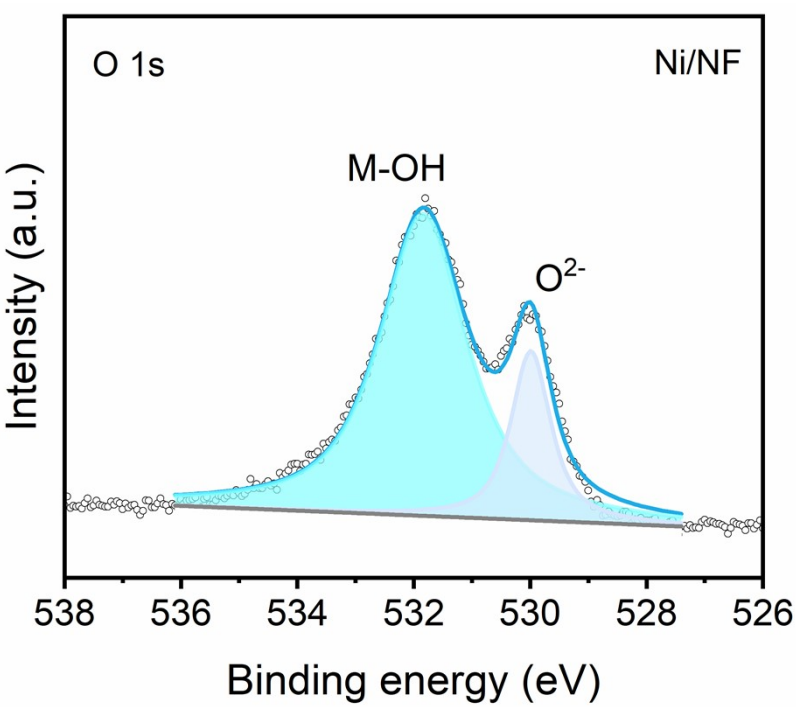

Figure S10. XPS O 1s spectra of Ni/NF.

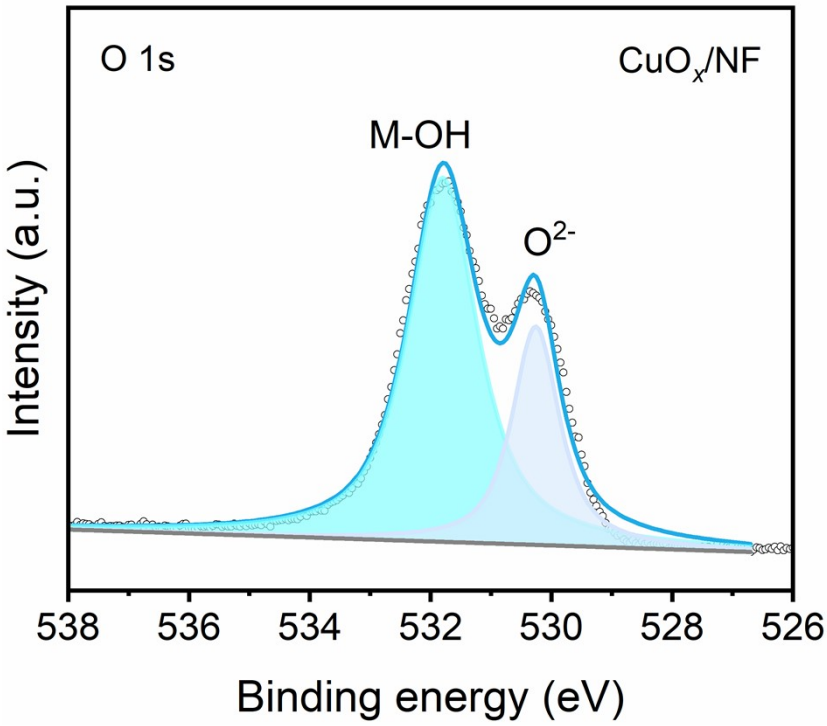

Figure S11. XPS O 1s spectra of CuO_x/NF.

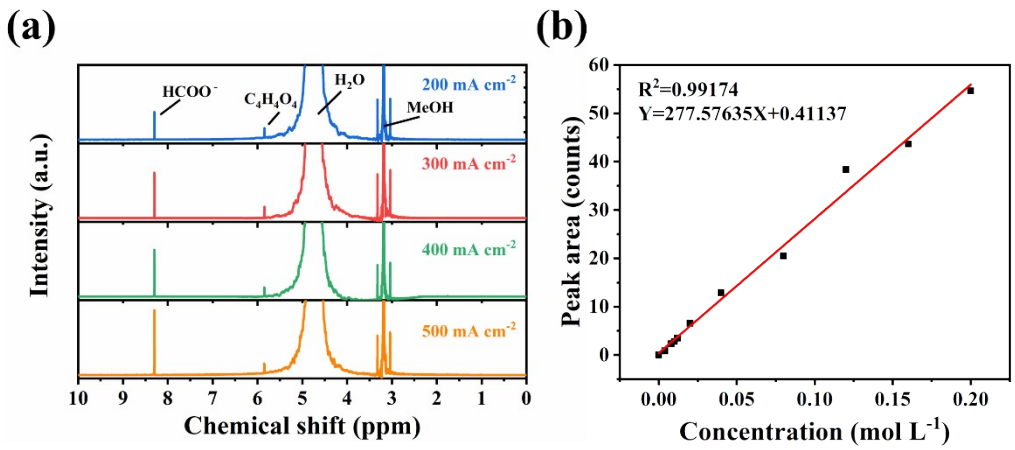

Figure S12. (a) ^{1}H NMR measurements of methanol oxidation to formate on anode at 200, 300, 400, 500 mA cm^{-2} in 1.0 M KOH solution with 1.0 M methanol addition. (b) The measured formate amount and theoretical values on anode.

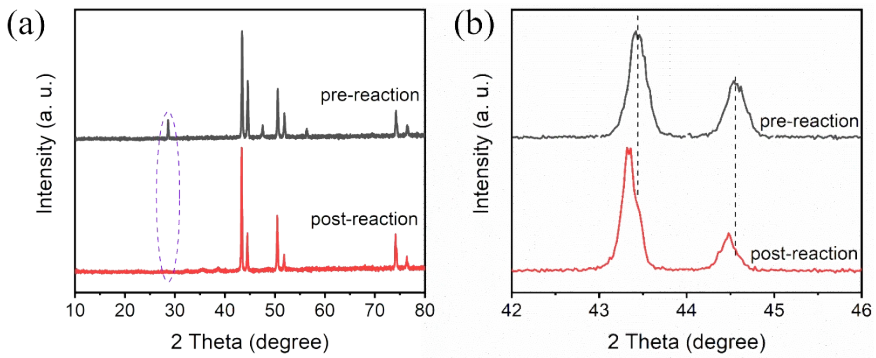

Figure S13. (a) The comparisons of XRD patterns for $NiCuO_x$-2/NF before and after the stability tests. (b) The enlarged XRD patterns in the range of 42-46°.

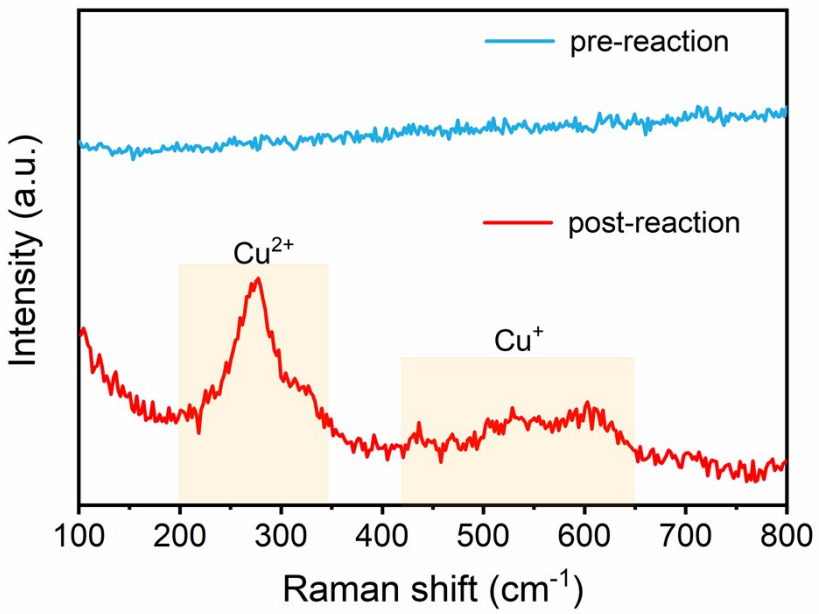

Figure S14. The comparisons of Raman spectra for $NiCuO_x$-2/NF before and after the stability tests.

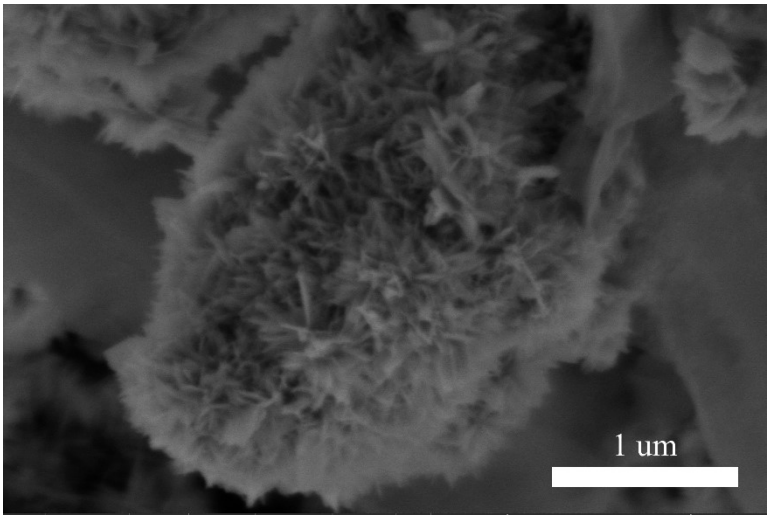

Figure S15. The SEM image of $NiCuO_x$-2/NF after the stability test.

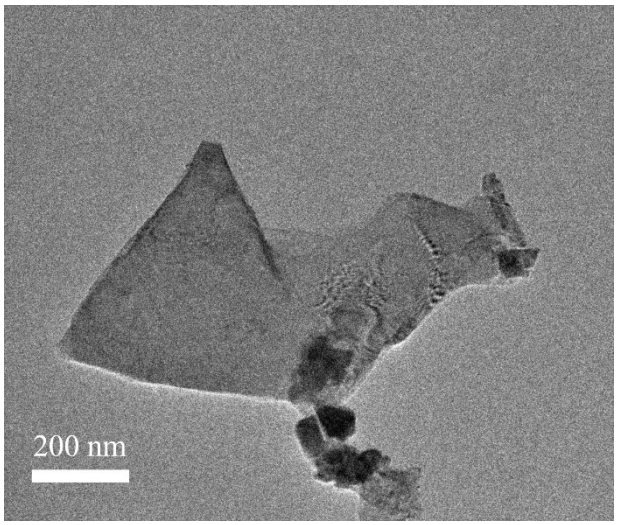

Figure S16. The TEM image of $NiCuO_x$-2/NF after the stability test.

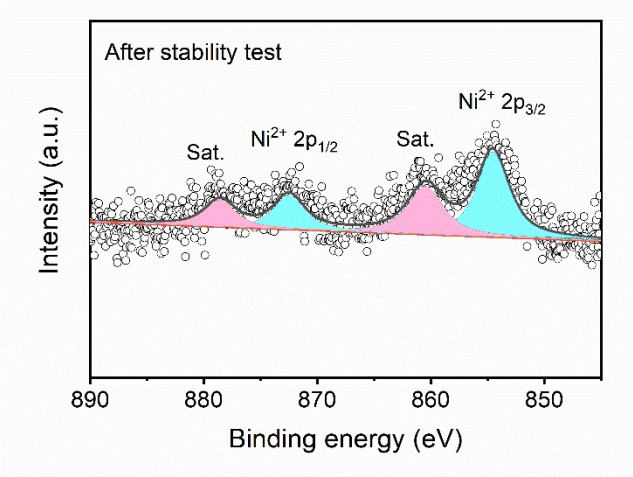

Figure S17. The XPS Ni 2p result of $NiCuO_x$-2/NF after the stability test.

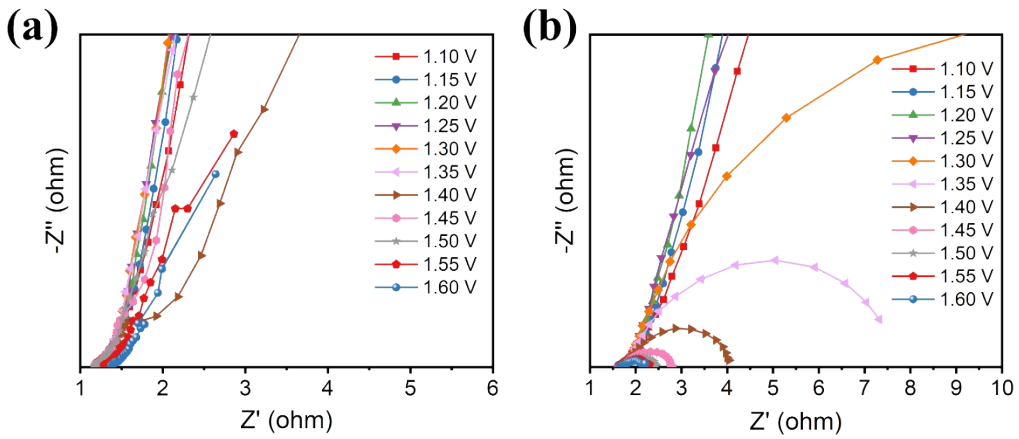

Figure S18. Nyquist plots of $NiCuO_x$-2/NF in (a) OER and (b) MOR.

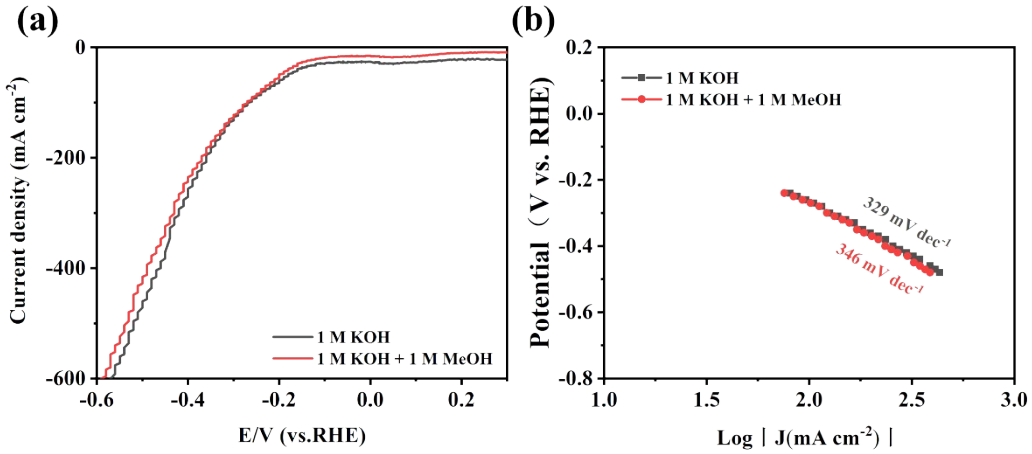

Figure S19. LSV curves of $NiCuO_x$-2/NF toward HER (a) and the corresponding Tafel plots (b).

Table S1. The specific data about Ni and Cu content for $NiCuO_x$ in TEM-EDS results.

Sample	Ni (at. %)	Cu (at. %)	Ni/Cu ratio
$NiCuO_x$-1	5.12	40.79	0.13
$NiCuO_x$-2	5.64	57.93	0.1
$NiCuO_x$-3	3.44	70.25	0.05

Table S2. The specific data about Ni and Cu content for $NiCuO_x$ in XPS results.

Sample	Ni (at. %)	Cu (at. %)	Ni/Cu ratio
$NiCuO_x$-1	4.14	32.2	0.13
$NiCuO_x$-2	2.87	32.31	0.09
$NiCuO_x$-3	1.19	29.07	0.04

Table S3. The comparisons between $NiCuO_x$-2/NF and other reported self-supporting Ni-based MOR catalysts.

Catalyst	Electrolyte	Activity	Duration time (h)	Corresponding current density (mA cm^{-2})	Reference
NiP_x-R/NF	1 M KOH + 0.5 M MeOH	1.40 V for 400 mA cm^{-2}	1	250	1
$Ni(OH)_2$/NF	1 M KOH + 0.5 M MeOH	1.36 V for 100 mA cm^{-2}	15	20	2
LC-$Ni(OH)_2 \cdot xH_2O$/NF	1 M KOH + 0.5 M MeOH	1.43 V for 200 mA cm^{-2}	28	130	3
CNFs@NiSe/CC	1 M KOH + 1 M MeOH	1.55 V for 400 mA cm^{-2}	2	300	4
S-NiCo-LDH/NF	1 M KOH + 1 M MeOH	1.41 V for 400 mA cm-^{2}	11	100	5
Ru&Fe-WO_x/NF	1 M KOH + 3 M MeOH	1.51 V for 500 mA cm^{-2}	28	200	6
NiIr-MOF/NF	1 M KOH + 4 M MeOH	1.41 V for 100 mA cm^{-2}	20	10	7
Ni-NF	1 M KOH + 0.5 M MeOH	1.388 V for 500 mA cm^{-2}	5	100	8

$Ni_{0.33}Co_{0.67}(OH)_2$/NF	1 M KOH + 0.5 M MeOH	1.33 V for 10 mA cm^{-2}	20	30	9
Co_xP@NiCo-LDH/NF	1 M KOH + 0.5 M MeOH	1.34 V for 100 mA cm^{-2}	20	45	10
t-NiCo-MOF/NF	1 M KOH + 0.5 M MeOH	1.4 V for 698 mA cm^{-2}	11	100	11
Fe-NF-500	1 M KOH + 1 M MeOH	1.472 V for 600 mA cm^{-2}	40	300	12
NiMn-LDH/NF	1 M KOH + 3 M MeOH	1.49 V for 500 mA cm^{-2}	20	100	13
Ni_3S_2-CNFs/CC	1 M KOH + 1 M MeOH	1.74 V for 1000 mA cm^{-2}	3	700	14
Mo-Co_4N/CC	1 M KOH + 3 M MeOH	1.356 V for 10 mA cm^{-2}	60	10	15
h-NiSe/CNTs	1 M KOH + 1 M MeOH	1.91 V for 400 mA cm^{-2}	20	350	16
$Co(OH)_2$@HOS/CP	1 M KOH + 3 M MeOH	1.53 V for 100 mA cm^{-2}	20	10	17
$NiCuO_x$-2/NF	1 M KOH + 1 M MeOH	1.42 V for 500	600	500	This work

		mA cm^{-2}			

References:

[1] S. Li, R. Ma, J. Hu, Z. Li, L. Liu, X. Wang, Y. Lu, G.E. Sterbinsky, S. Liu, L. Zheng, J. Liu, D. Liu, J. Wang, Coordination environment tuning of nickel sites by oxyanions to optimize methanol electro-oxidation activity, Nat. Commun., 13 (2022) 2916.

[2] J. Hao, J. Liu, D. Wu, M. Chen, Y. Liang, Q. Wang, L. Wang, X.-Z. Fu, J.-L. Luo, In situ facile fabrication of $Ni(OH)_2$ nanosheet arrays for electrocatalytic co-production of formate and hydrogen from methanol in alkaline solution, Appl. Catal. B, 281 (2021).

[3] G. Fu, X. Kang, Y. Zhang, X. Yang, L. Wang, X.Z. Fu, J. Zhang, J.L. Luo, J. Liu, Coordination Effect-Promoted Durable $Ni(OH)_2$ for Energy-Saving Hydrogen Evolution from Water/Methanol Co-Electrocatalysis, Nano-micro Lett., 14 (2022) 200.

[4] B. Zhao, J.-W. Liu, Y.-R. Yin, D. Wu, J.-L. Luo, X.-Z. Fu, Carbon nanofibers@NiSe core/sheath nanostructures as efficient electrocatalysts for integrating highly selective methanol conversion and less-energy intensive hydrogen production, J. Mater. Chem. A, 7 (2019) 25878-25886.

[5] C. Xiao, L. Cheng, Y. Wang, J. Liu, R. Chen, H. Jiang, Y. Li, C. Li, Low full-cell voltage driven high-current-density selective paired formate electrosynthesis, J. Mater. Chem. A, 10 (2022) 1329-1335.

[6] Q. Yang, C. Zhang, B. Dong, Y. Cui, F. Wang, J. Cai, P. Jin, L. Feng, Synergistic modulation of nanostructure and active sites: Ternary Ru&Fe-WO_x electrocatalyst for boosting concurrent generations of hydrogen and formate over 500 mA cm^{-2}, Appl. Catal. B, 296 (2021).

[7] Y. Xu, M. Liu, M. Wang, T. Ren, K. Ren, Z. Wang, X. Li, L. Wang, H. Wang, Methanol electroreforming coupled to green hydrogen production over bifunctional NiIr-based metal-organic framework nanosheet arrays, Appl. Catal. B, 300 (2022).

[8] C. Cao, D.D. Ma, J. Jia, Q. Xu, X.T. Wu, Q.L. Zhu, Divergent Paths, Same Goal: A Pair-Electrosynthesis Tactic for Cost-Efficient and Exclusive Formate Production by Metal-Organic-Framework-Derived 2D Electrocatalysts, Adv. Mater., 33 (2021) e2008631.

[9] M. Li, X. Deng, K. Xiang, Y. Liang, B. Zhao, J. Hao, J.L. Luo, X.Z. Fu, Value-Added Formate Production from Selective Methanol Oxidation as Anodic Reaction to Enhance Electrochemical Hydrogen Cogeneration, ChemSusChem, 13 (2020) 914-921.

[10] M. Li, X. Deng, Y. Liang, K. Xiang, D. Wu, B. Zhao, H. Yang, J.-L. Luo, X.-Z. Fu, Co P@NiCo-LDH heteronanosheet arrays as efficient bifunctional electrocatalysts for co-generation of value-added formate and hydrogen with less-energy consumption, J. Energy Chem., 50 (2020) 314-323.

[11] X. Deng, M. Li, Y. Fan, L. Wang, X.-Z. Fu, J.-L. Luo, Constructing multifunctional 'Nanoplatelet-on-Nanoarray' electrocatalyst with unprecedented activity towards novel selective organic oxidation reactions to boost hydrogen production, Appl. Catal. B, 278 (2020).

[12] Y. Hao, D. Yu, S. Zhu, C.-H. Kuo, Y.-M. Chang, L. Wang, H.-Y. Chen, M. Shao, S. Peng, Methanol upgrading coupled with hydrogen product at large current density promoted by strong interfacial interactions, Energy Environ. Sci., 16 (2023) 1100-1110.

[13] B. Zhu, B. Dong, F. Wang, Q. Yang, Y. He, C. Zhang, P. Jin, L. Feng, Unraveling a bifunctional mechanism for methanol-to-formate electro-oxidation on nickel-based hydroxides, Nat. Commun., 14 (2023) 1686.

[14] B. Zhao, J. Liu, X. Wang, C. Xu, P. Sui, R. Feng, L. Wang, J. Zhang, J.-L. Luo, X.-Z. Fu, CO_2-emission-free electrocatalytic CH_3OH selective upgrading with high productivity at large current densities for energy saved hydrogen co-generation, Nano Energy, 80 (2021).

[15] T. Wang, X. Cao, H. Qin, X. Chen, J. Li, L. Jiao, Integrating energy-saving hydrogen production with methanol electrooxidation over Mo modified Co_4N nanoarrays, J. Mater. Chem. A, 9 (2021) 21094-21100.

[16] B. Zhao, J. Liu, C. Xu, R. Feng, P. Sui, L. Wang, J. Zhang, J.L. Luo, X.Z. Fu, Hollow NiSe Nanocrystals Heterogenized with Carbon Nanotubes for Efficient Electrocatalytic Methanol Upgrading to Boost Hydrogen Co-Production, Adv. Funct. Mater., 31 (2020).

[17] K. Xiang, D. Wu, X. Deng, M. Li, S. Chen, P. Hao, X. Guo, J.L. Luo, X.Z. Fu,

Boosting H_2 Generation Coupled with Selective Oxidation of Methanol into Value-Added Chemical over Cobalt Hydroxide@Hydroxysulfide Nanosheets Electrocatalysts, Adv. Funct. Mater., 30 (2020).